IEEE Photonics Journal
An IEEE Photonics Society Publication

Open Access

Enhanced Frequency-Upconverted Photoluminescence and Terahertz Emission From Graphene

Volume 9, Number 3, June 2017

Ken Liu
Quan Guo
Jian Fa Zhang
Zhi Hong Zhu
Chu Cai Guo
Shi Qiao Qin

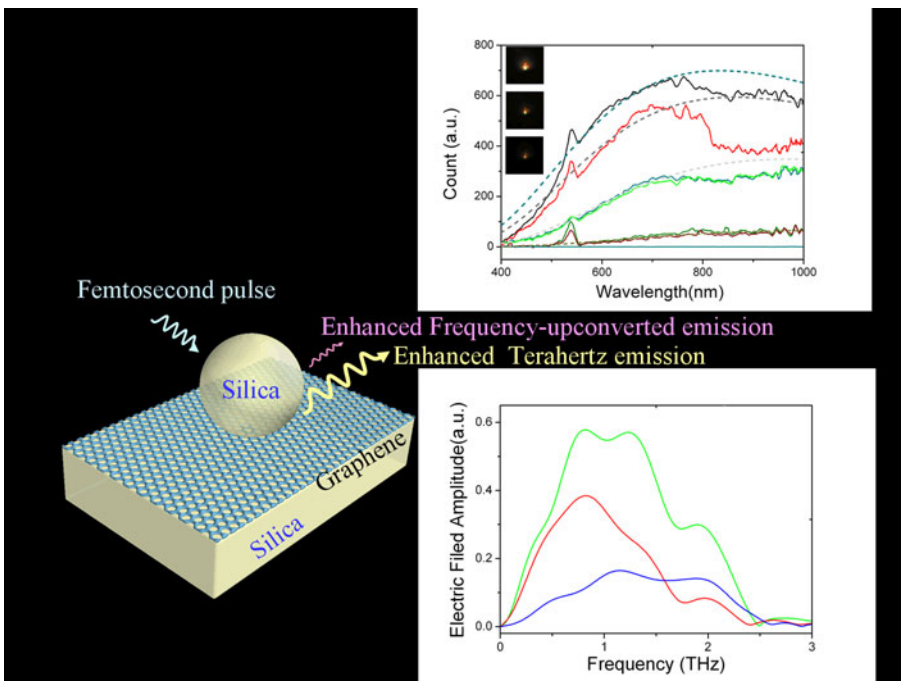

DOI: 10.1109/JPHOT.2017.2691261
1943-0655 © 2017 IEEE

IEEE photonics SOCIETY

IEEE

Enhanced Frequency-Upconverted Photoluminescence and Terahertz Emission From Graphene

Ken Liu,[1] Quan Guo,[2] Jian Fa Zhang,[1] Zhi Hong Zhu,[1] Chu Cai Guo,[1] and Shi Qiao Qin[1,3]

[1]College of Optoelectronic Science and Engineering, National University of Defense Technology, Changsha 410073, China
[2]College of Science, National University of Defense Technology, Changsha 410073, China
[3]State Key Laboratory of High Performance Computing, National University of Defense Technology, Changsha 410073, China

DOI:10.1109/JPHOT.2017.2691261

Manuscript received February 23, 2017; revised March 18, 2017; accepted March 29, 2017. Date of publication April 5, 2017; date of current version April 25, 2017. This work was supported in part by the National Natural Science Foundation of China under Grant 61404174, Grant 11674396, Grant 11304389, Grant 11374367, and Grant 61205087 and in part by the National University of Defense Technology Foundation under Grant ZK16-02-01. Corresponding author: Ken Liu (e-mail: liukener@163.com).

Abstract: Graphene is a gapless material with a linear energy–momentum dispersion relationship. Because of its unique band structure, graphene has been demonstrated as an ultra-broadband photon absorption material from the visible to terahertz frequency ranges. Here, we study the reverse process: photon emission from graphene. Using silica microsphere structures and femtosecond laser pulse excitation, photon emission enhancement at visible, near infrared, and terahertz ranges were achieved. These results help to promote graphene as a new type of light generation material, which can overcome the restriction that the emission wavelength is determined by the material bandgap. It is also found that the graphene's electrical properties, such as the nonlinear conductivity, changed significantly with the enhancement of the absorption during the ultrafast process.

Index Terms: Ultrafast optics, ultrafast nonlinear processes, THZ optics.

1. Introduction

Light generation from conventional semiconductor materials depends heavily on its associated band structure [1]. Indirect bandgap materials, such as silicon, have low emission efficiency [2]–[5]. This is a result of the photons having a negligibly small momentum compared to that of electrons, so that the momentum conservation cannot be satisfied with electron-hole pair recombination from the minimum of the conduction band and maximum of the valence band for indirect bandgap materials. Only a limited set of semiconductor materials that have direct gaps in e-k space can be used for practical light generation applications [1]. For these materials, the desired emission wavelength is determined by the bandgap of the material, and the materials only emit at a certain wavelength range. While quantum cascade laser could engineer gap energy of intersub-band for light emission, they need complicated fabrication processes. Thus, in most cases, different materials were chosen for different desired emission wavelengths.

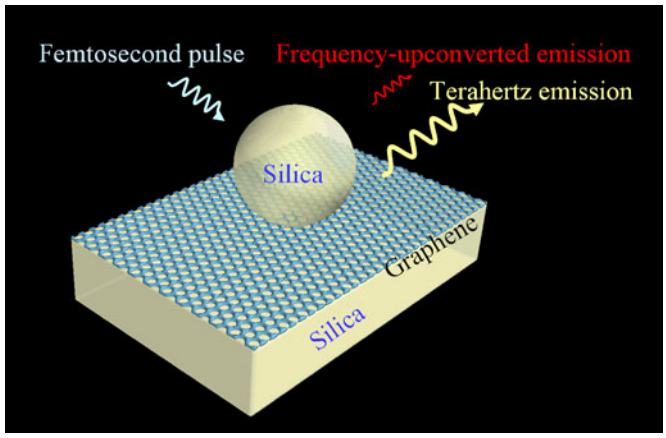

Fig. 1. Schematic of enhanced photon emission from graphene. A silica microsphere is placed above graphene sheets on a silica substrate. The angle of incidence is 45°.

Graphene is a gapless material with a linear and symmetrical energy-momentum dispersion relationship [6]. Based on this unique band structure, broadband optical absorption from the visible to terahertz ranges has been demonstrated in graphene [7]–[13]. The reverse process, photon emission from graphene, exhibits extremely low emission efficiency [14]–[18]. This is because that in graphene, the optical radiative recombination rate is much lower than the hot carrier relaxation rate. After optical injections in graphene, almost all of the hot carriers in graphene relax to thermal equilibrium states. To increase the emission efficiency, one can decrease the hot carrier relaxation rate such as reducing the thermal conductivity of graphene [19]. In the experiment [19], the emission is in agreement with thermal radiation from graphene. While for doped graphene integrated on silicon waveguide, the emission spectra does not show a typical thermal radiation property [20], which suggests a different emission mechanism. In this paper we show that the emission efficiency can also be increased by increasing the electron-hole recombination rate. The spontaneous radiative recombination rate can be written as $R_{sp} = A_{21}N_2$, where A_{21} are the Einstein coefficients, N_2 is the number of electron-hole pair states, which suggests that the upper state is full and the lower state is empty. Here, we find that R_{sp} can be enhanced by increasing N_2. Furthermore, N_2 rises with the field enhancement. In this paper, we show the increase of R_{sp} following the increase in the field enhancement achieved using silica microspheres covering the graphene.

2. Field Enhancement With Silica Microspheres

Graphene is an ultra-thin material. For normal incidence, the photon-graphene interaction length is equal to the thickness of the graphene [18], [21], which limits the photon-graphene interaction effects. To increase the photon-graphene interaction, field enhancement structure designed is shown in Fig. 1. Few-layer (3∼5 layers) graphene was placed on a crystalline silica (quartz) substrate, and silica microspheres were deposited on top of the graphene. Femtosecond laser pulses at approximate wavelengths of 1590 and 800 nm were used to excite the frequency-upconverted photoluminescence and THz emission, respectively.

For an incident plane wave, there are two types of modes that can be classified: the transverse magnetic (TM) mode incidence with the magnetic field in the x-y plane and transverse electric (TE) mode incidence with the electric field in the x-y plane. Because the scattering electrical field, E_z, is perpendicular to the graphene surface, it does not contribute to the in-plane current of the graphene. As a result, we do not consider the E_z scattering component in this work. For the incident TM mode, the E_z scattering primarily resulted from the scattering of the z component of the incident electrical field E_{z-inc}. Hence for the incident TM mode, we only consider the y component of the incident

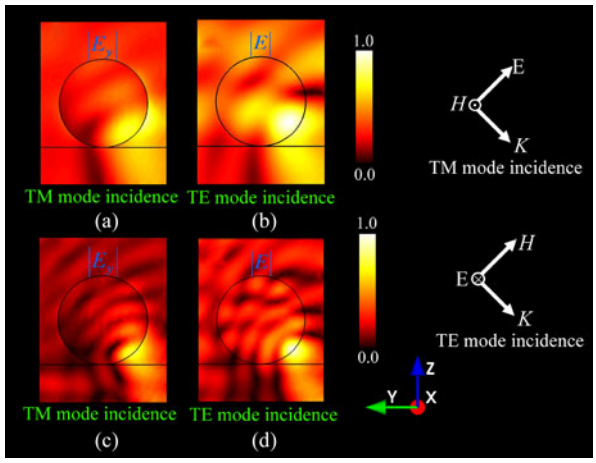

Fig. 2. Normalized scattering field distributions with a 45° incidence angle. The incident wavelengths are (a), (b) 1590 nm and (c), (d) 800 nm. (a) and (c) Scattering $|E_y|$ distribution for the incident TM mode plane wave. (b) and (d) Scattering $|\vec{E}|$ distribution for the incident TE mode plane wave.

electrical field E_{y-inc}, where $E_{y-inc} = E_{inc} \cos\theta$, and θ is the incident angle with respect to normal. The microsphere behaves like micro lens with the focal region located in the sphere opposite to where the incident light impacts. When θ was increased (e.g., 60°), the focal area moved away from the bottom of the sphere where graphene was located. While for a small θ (e.g. 0°), the microsphere did not behave like a good micro lens because the focal area was located at the silica substrate and both the microsphere and substrate have the same refraction index. Therefore, a 45° incident angle was chosen to balance these effects, as shown in Fig. 2.

Fig. 2 shows the scattering field with wavelengths at 1590 and 800 nm both for TM and TE modes. For the incident TE mode, there was no E_{z-inc} component, and the E_z scattering component at the microsphere/substrate interface was relatively weak. Thus, the field enhancement effect was better than that of the incident TM mode (see Fig. 2). It was observed that for the 800 and 1590 nm excitation wavelengths, the enhancement effect always exists and showed broadband field enhancement. This phenomenon is different from the structure using whispering gallery modes (WGM) to enhance light absorption in the layer far below the sphere [22]. No WGM effect was considered in our simulations. The WGM mode only enhances absorption of particular resonant modes, and the existence of WGM modes requires perfect spherical walls for the microsphere; however, any deform of the sphere could greatly decrease the quality factor of the mode. Thus, WGM modes require a high-precision three dimensional fabrication at micrometer scale.

3. Results and Discussion

3.1 Material and Method

The intrinsic graphene used in this paper was approximately three to five layers thick. Graphene was grown on copper foils by CVD and the as-grown graphene is multi-layer. After being spin-casted onto PMMA, copper was dissolved using a solution. The graphene with PMMA was transferred to water and then to the silica substrate, and finally the PMMA layer was dissolved by acetone solution. Then, silica microspheres with diameters of 1400 nm are used for covering on graphene, which were left to dry in ambient conditions. The microspheres were randomly dispersed on the graphene. A femtosecond laser with a center wavelength of 1590 nm was coupled to a single mode fiber. The tip of the fiber was etched as a micro-lens, and the light intensity has a Gaussian profile in the focal area with a diameter of approximately 4 μm. For 45° incident angle, the focal area was estimated to be 6 μm on silica substrate. Since the size of the focal area is larger than the size of one microsphere, we focus the pulse on the area A and area B with seven microspheres

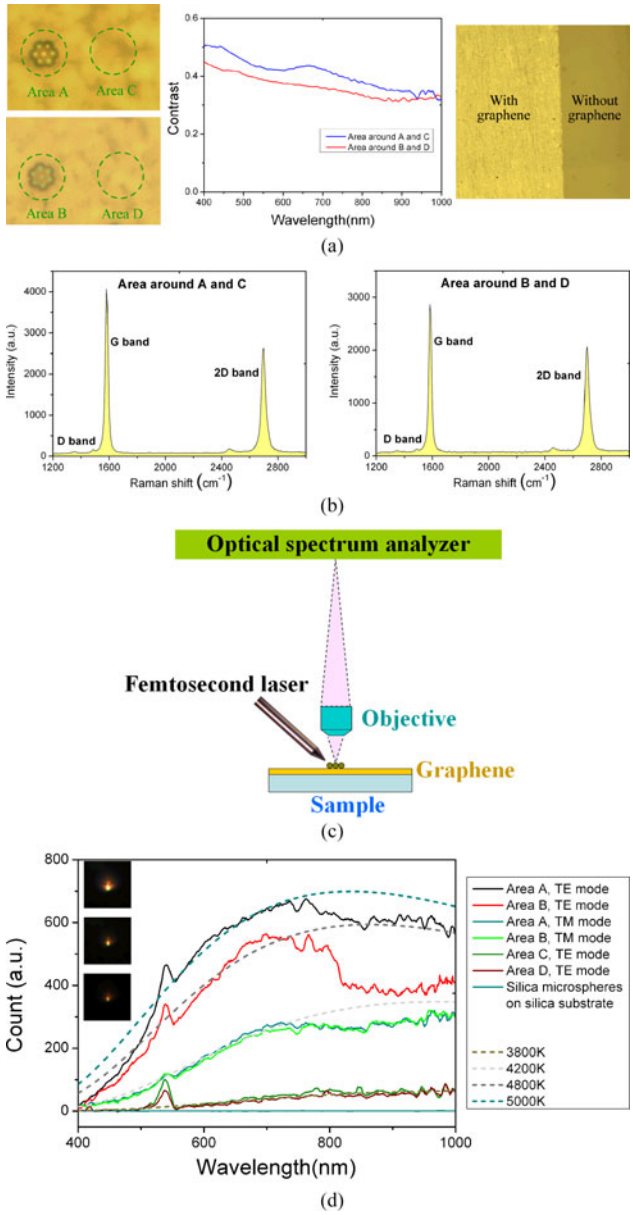

Fig. 3. (a) Experimental contrast of the reflectance from three to five layers graphene on silica substrate and the reflectance from bare silica substrate without graphene. Left two figures shows four different areas captured with CCD camera. Area A and B are areas where seven microspheres gathered together, as illustrated in Fig. 1. Area C and D are areas a few microns away from A and B and consist of graphene on silica substrate, but they do not have the coverage of microspheres. The reflectance was measured from area near area A (blue line) and near area B (red line). The right figures shows the optical image of graphene on silica substrate. (b) Raman spectra of the graphene near area A and area B. (c) Schematic of the frequency-upconverted photoluminescence from graphene sample experiment setup. (d) Photoluminescence and THG spectra of graphene. Lines are experimentally measured results at different areas. Short dashed lines are theoretically calculated emission at different temperatures. Measurements were taken, and light was focused on different areas and materials. The curve for "Silica microspheres on silica substrate" was measured from area region that contained microspheres on the silica substrate without coverage of graphene. (Insets) Photoluminescence emission photos captured with a CCD camera. From top to bottom, they are the emission photo from Area A, with TE and TM modes polarization incidence, and the emission photo from Area C. All of the emission spectra have the same integration time from the optical spectra analyzer, and was normalized by CCD spectral response.

for photoluminescence enhancement measurement, which were shown in Fig. 3(a). The graphene layer thickness near area A and area B can be determined by optical reflectance contrast of silica substrate with graphene and without graphene, and the method works well for few layer graphenes as a function of thickness [8], [11]. The contrast can be written as Contrast(λ) $=\frac{R_{g+s}-R_s}{R_s} = \frac{4}{n_s^2-1}A$, where R_{g+s} and R_s are the reflected lights from the graphene on silica substrate and bare silica substrate respectively, n_s is the refraction index of the silica substrate, A is the graphene absorbance. A $\approx$ 2.3% for monolayer graphene, and $n_s^2 \approx 2.0$ for quartz substrate. A $\approx$ 9.2% and 7.5% near Area A and Area B respectively. In Fig. 3(b), the Raman spectra also show that the intensity ratios I(G)/I(2D) are about 1.5 and 1.4 near Area A and Area B,respectively. Comparing the reflection results with reference [11] and Raman spectra with reference [23], the graphene is about 3.3–4.0 atomic layers.

For THz radiation measurements, we used a femtosecond laser with an average output power of 650 mW to excite the THz emission. The emitted THz electrical signal was detected by a 1.0 mm thick ZnTe crystal, and this is a standard THz time-domain spectroscopy setup. Since THz detection system is more sensitive to 800 nm lasers, we use the excitation laser with the center wavelength approximately 800 nm, a pulse width of approximately 150 femtoseconds and a repetition rate of 60 MHz (Mira900). The incident angles of the excitation pulse were 45°. For visible and near infrared photoluminescence excitation, the femtosecond laser has an output power of 10 mW at the fiber tip. The center wavelength is about 1590 nm, the pulse width is about 130 femtoseconds, and the repetition rate is 100 MHz (Menlo systems C-Fiber). The Mira900 laser has an output energy about 2 orders larger than that of the Menlo laser, which could help to increase the THz emission intensity.

3.2 Enhanced Visible and Near Infrared Light Emission

As shown in Fig. 3(c), to measure the photoluminescence of graphene, the ultrafast pulse was first used to excite the photoluminescence of the silica substrate, but no corresponding signal was detected by the optical spectrum analyzer (OSA). We then used the ultrafast pulse to excite the photoluminescence of the silica spheres on top of the bare silica substrate, as shown in Fig. 3(d). We found that the photoluminescence signal of silica spheres with a diameter of 1400 nm did not reach the threshold of the OSA detector. Therefore, in the following measurement, we determined that the observed photoluminescence effect was not a result of the silica microspheres/silica substrate. Then, we performed measurements on the dispersed microspheres. Because the diameter of the focus was approximately 6 μm, we focalized the pulse to four different areas, as shown in Fig. 3(a). Area A and B are areas where seven microspheres gathered together. The sizes of Area A and B were comparable to the focal area of the injection pulse. A few microns to the side of Area A and B were Area C and D, where graphene was located on silica substrate but had no silica microspheres on top. We used the pulse to excite the bare graphene located at Area C and D to obtain the emission spectra. The spectra contains two components: frequency-upconverted photoluminescence and third harmonic generation (THG). The frequency-upconverted photoluminescence from bare graphene/silicon can be subjected to thermal radiation of hot electrons in graphene, which is consistent with the analyses in the previous paper [14], and the effective emission temperature T is about 3800 K.

To achieve emission enhancement as analyzed above, we coupled the injection pulse for Area A and B. From Fig. 3(d), we found that the photoluminescence was consistent with our predictions. The ordinates of the emission spectra show the emission photon numbers detected by OSA. Thus the emission enhancement can be estimated by the area size below the emission spectra curve. As an estimation of the area size, we can deduce that the emission was enhanced approximately five times by the TM mode injection and approximately one order by the TE mode injection. As shown in Fig. 3(d), for field enhancement structures, the emission spectra do not agree well with the thermal radiation properties. The emission disagreement can be explained from the hot electron linear scattering process [20]. If no hot electron-hole pairs are generated and the number of hot carriers does not increase, the process can be regard as hot carrier scattering, and electrons will

collide with states of higher energy. If in the process the net number of hot electrons increases, the process can be regard as hot carrier multiplication. All the process can be regarded as Auger process. With the electrical field enhancement as analyzed from Fig. 2, the total photo-excited hot electron-hole pairs N_2 increased, which could lead to an increased photo emission rate because $R_{sp} = A_{21}N_2$. The hot carrier scattering and hot carrier multiplication could cause the emission increase more quickly at high frequency than that at low frequency, which has been shown in Fig. 3(d). The emission decreases at low frequency when compared with the thermal radiation.

Studies about pump-probe spectroscopy with graphene show that carrier multiplication should be the fundamental mechanism in graphene [24], [25]. While in another study [26], by a direct map of transient occupation of electronic states, researchers obtain opposite conclusion that there is no carrier multiplication in graphene. As shown in Fig. 3(d), for the effective emission temperature T = 3800 K [14], the emission still exhibits thermal radiation properties, without indication of hot carrier multiplication. After increasing the injection intensity at the graphene surface, more electrons in valence band are pumped to the conduction band. In this case, the Auger process becomes obvious during the hot carrier relaxation. The electrons in higher energy states collide with electrons in states of lower energy, and the result is that more electrons appear in a mean energy states. This is why the emission peaks appear at 600–800 nm, and there are mismatch at the wavelength longer than 800 nm and shorter than 600 nm. The mismatch indicates the linear scattering process such as hot carrier multiplication and hot carrier scattering. The results indicate that linear scattering process indication can only be found with intense pump, thus the mechanism of carrier multiplication may not be applied in graphene for light harvesting in solar cells. There is a little emission difference for TE modes incidence at different areas A and B. This is because that in the emission enhancement experiment, the emission is very sensitive to the light coupling between the tapered fiber tip and sample. Hence the coupling difference caused the emission difference as shown in Fig. 3(d). Insets in Fig. 3(d) shows the CCD captured photos. The excitation intensity has a Gaussian profile in real space. But the incident angle is 45°, the excitation intensity at the area is not homogenous. Thus, emission pattern from the focus area is not homogenous.

3.3 Third Order Conductivity Change of the Graphene

Previous studies have shown that graphene has an ultra-large nonlinear coefficient such as Kerr coefficient 5∼6 orders larger than that of silicon in the communication wavelength range [21], [27]–[29]. At 1590 nm, the Kerr coefficient of graphene was approximately six orders larger than that of silicon and 8 orders larger than that of silica [29]. Here, we can also find that the multi-layer graphene had a much stronger THG than that from bulk silica materials. Before transferring graphene to silica substrate, there was no THG signal from the bare silica substrate. After transferring graphene to the silica substrate, THG signal emitted at about 530 nm together with frequency-upconverted photoluminescence (olive and wine lines in Fig. 3(d)). The THG intensity was stronger than that of the photoluminescence. However following the excitation electrical field increase and the graphene photoluminescence enhancement, the THG emission intensities do not increase. The previous theoretical nonlinear optical analyses from graphene were performed in thermal equilibrium [21], [27]–[29], but the real THG processes were in non-thermal equilibrium, especially considering the photoluminescence. In the field enhancement cases, the absorption of photons in graphene for the ultrafast cases would induce an electronic band change and produce a significant amount of phonons resulting in carrier-phonon scattering. The existence of these phonons affects the conductivity of graphene. The electron collision rate is primarily determined by the electron-phonon interaction, and the existence of excess phonons could increases the resistivity of graphene. Thus, the conductivity including the first and higher order conductivities, such as third order conductivity, should decrease sharply during the ultrafast process. As a result, while the excitation light intensity increased, the THG does not increase. Another recent experiment shows that the thermal conductivity of graphene at high temperatures is also greatly reduced [19]. The thermal conductivity reduction induces more phonons generation and a further electrical conductivity reduction, the electrical conductivity reduction induces more hot electrons generation and a further thermal

conductivity reduction. Both the thermal conductivity and electrical conductivity reduce simultaneously. It should be noticed that in the ultrafast process, the band structure of graphene has been greatly changed, this would also change the nonlinear property of graphene.

3.4 Enhanced Terahertz Emission

To measure the THz emission from graphene, we use femtosecond laser with a power of 11 nJ per pulse and a center wavelength at approximately 800 nm for excitation, with a Gaussian profile in time domain and pulse width of approximately 150 femtoseconds. To collect the THz emission efficiently, the focal area diameter was adjusted to approximately 500 μm, with Gaussian profile of light intensity in real space. Because the focal size in the THz excitation is much larger than that in the photoluminescence experiment shown in Fig. 3, two graphene excitation area E and area F with different dispersed density were used to excite the THz emission. Hence, different graphene areas have different THz emission intensities. Fig. 4(a) shows the schematic of the experiment setup. Fig. 4(b) and (c) show the THz emission spectra from bare graphene on a silica substrate and graphene covered with silica microspheres. The figure confirms that there was THz emission from graphene. With the microspheres, the THz emission amplitude from graphene was also enhanced several times. The THz emission from graphene was explained by stimulated emission of hot carriers in population inversion states [30], [31] or by photon drag currents in graphene [32]–[34]. Here we found that the THz generation in graphene may be more complicated. In surface plasmon enhanced THz emission experiments, only the TM mode of the THz electric field can be enhanced, and without plasmon, there is polarization change of the THz electric field [32]. But Fig. 3(d) shows the experimental measured polarized THz emission intensity v.s the polarization angle of the incident beam. There is no polarity change of THz wave Ey component, and this can not be explained by the "photon drag current" effect [32]. Recent experiments have demonstrated the generation of photocurrent from graphene after optical absorption [12]–[13]. The observed THz generation may be a result of the ultrafast photocurrent generation. Hot electron emission from gold nano-structures has previously been observed with an ultrafast pump [35]. The non-equilibrium hot electrons could be injected into the graphene structure, thus effectively changing the surface potential of the graphene nearby and enhancing photocurrent and THz emission [36]. Another interesting study shows that hot electron emission could also occur in graphene. The ejected electrons in graphene could provide more momentum than photons [37]. Thus THz generation may due to transient photoconductive current and photothermoelectric effects [38]. And recent study [39] manifests the occurrence of THz generation in graphene the acceleration of ultrafast photoexcited charge carriers in graphene in the presence of a dc electric field. If an intense excitation breaks the linear symmetric dispersion, carrier distributions in e-k space may be imbalanced, causing internal dc-electric fields. This may also become a factor that causes the THz radiation. Thus we found that the THz generation in graphene may be more complicated and need further study.

3.5 Discussions

From [22], light absorption in thin films below the substrate surface is enhanced by the WGM mode in the microsphere. In this paper, we did not observe the WGM enhancement effect. We think that this is because that the silica microsphere with diameter of 1.4 μm does not posses high quality factors, the deformation and the connection of the sphere with silica substrate would greatly decrease the quality factors. The low index silica spheres with micron-scale diameters correspond to lager bending loss. In this paper, we do not use periodic patterned spheres. The structure described in this paper can be fabricated, and broadband enhancement can be realized easily. The structure could also be used in other devices such as solar cells. However, field enhancement is primarily located at the area between the substrate surface and microsphere tip along the incident angle. This is because the microspheres can only act as micro lens being placed in low refractive index regions. The enhanced field cannot effectively penetrate through to the substrate with a high refractive index. Thus, the structure does not benefit light enhancement in the layer a few hundred

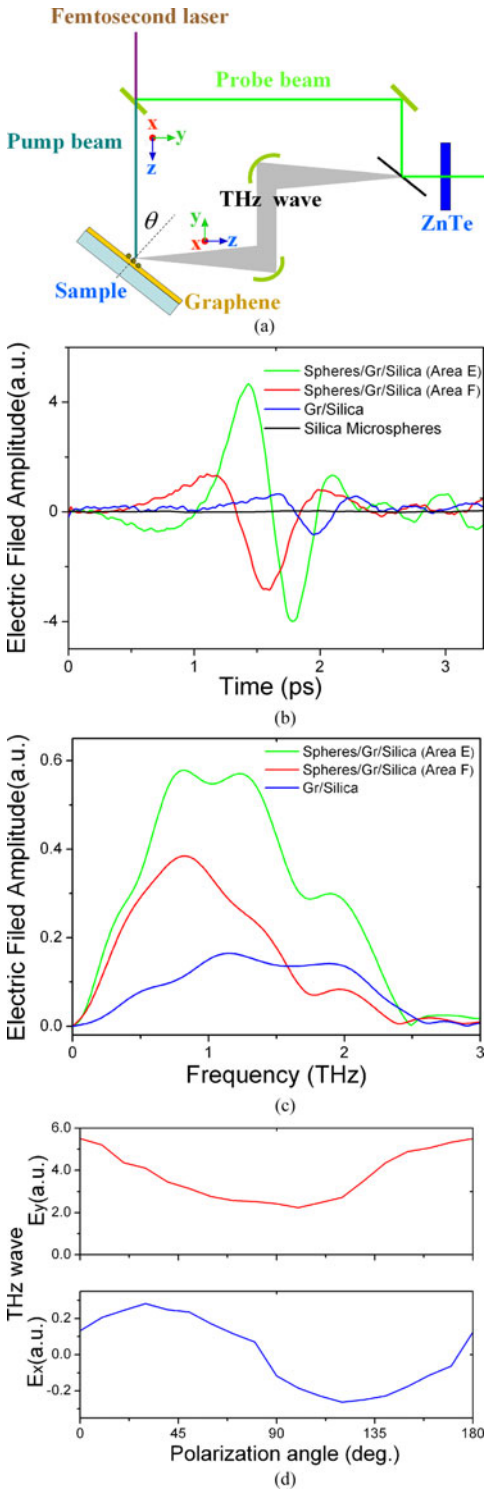

Fig. 4. THz emission from graphene. (a) Schematic of the THz wave generation and detection experiment setup. (b) THz electrical field variation in the time domain. (c) THz emission amplitude in the frequency domain. Area E and F are graphene areas covered with silica microspheres. (d) Experimental measured Ex and Ey components of the generated THz wave amplitudes, depending on the incident polarization angle, and here $\theta = 45°$.

nanometers below the substrate surface. Instead, the structure helps to achieve light enhancement at a layer on the substrate surface.

There are many methods that could achieve field enhancement other than the mechanisms described in this paper. That is, metallic nanostructures or nanoparticles also have strong electric field enhancements and can increase the fluorescence [40], but THG and frequency-upconverted photoluminescence in gold nanoparticles also exist [41], which can not be filtered from the graphene THG and photoluminescence. In this paper, in order to study the pure THG and photoluminescence from graphene, we do not use metallic nanostructures.

The Fermi level of the intrinsic graphene can be changed by substrate doping effect. This does not affect the frequency-upconverted photoluminescence, since the excitation and the emission photon energies are much larger than substrate doping induced Fermi level change. The Fermi level effects on the THz emission is not well studied in this paper, since the Fermi level of the graphene samples we used are fixed and can not be changed. In further study, to study the Fermi level effect on THz emission emission we would like to used electrically doped samples so that we can study the THz emission at various Fermi level.

4. Conclusion

We used silica microspheres to enhance the visible, near infrared, and THz emissions from graphene. The results help us to understand graphene as an ultra-broad band light generation material, without considering the band gap opening in graphene [42]. The emission spectra also gave the indication of carrier multiplication in graphene. Following the generation of a significant amount of hot carriers in graphene, the electrical properties, such as third-order susceptibility, which is dependent on the third-order conductivity, changes rapidly. This provides the opportunity of ultrafast tuning of nonlinear optical parameters of graphene.

Acknowledgment

The authors thank H. Luo for measurement preparation.

References

[1] L. A. Coldren and S. W. Corzine, *Diode Lasers Photonic Integrated Circuits*. New York, NY, USA: Wiley, 1995, pp. 9–12.
[2] B. Corcoran *et al.*, "Green light emission in silicon through slow-light enhanced third-harmonic generation in photonic crystal waveguides," *Nature Photon.*, vol. 3, pp. 206–210, 2009.
[3] W. D. A. M. de Boer *et al.*, "Red spectral shift and enhanced quantum efficiency in phonon-free photoluminescence from silicon nanocrystals," *Nature Nanotechnol.*, vol. 5, pp. 878–884, 2010.
[4] A. Shakoor *et al.*, "Enhancement of room temperature sub-bandgap light emission from silicon photonic crystal nanocavity by Purcell effect," *Physica B: Condens. Matter*, vol. 407, pp. 4027–4031, 2012.
[5] R. L. Savio *et al.*, "Room-temperature emission at telecom wavelengths from silicon photonic crystal nanocavities," *Appl. Phys. Lett.*, vol. 98, 2011, Art. no. 201106.
[6] A. H. Castro Neto, F. Guinea, N. M. R. Peres, K. S. Novoselov, and A. K. Geim, "The electronic properties of graphene," *Rev. Mod. Phys.*, vol. 81, pp. 109–162, 2009.
[7] R. R. Nair *et al.*, "Fine structure constant defines visual transparency of graphene," *Science*, vol. 320, pp. 1308–1308, 2008.
[8] K. F. Mak, M. Y. Sfeir, Y. Wu, C. H. Lui, J. A. Misewich, and T. F. Heinz, "Measurement of the optical conductivity of graphene," *Phys. Rev. Lett.*, vol. 101, 2008, Art. no. 196405.
[9] J. M. Dawlaty *et al.*, "Measurement of the optical absorption spectra of epitaxial graphene from terahertz to visible," *Appl. Phys. Lett.*, vol. 93, 2008, Art. no. 131905.
[10] L. Ren *et al.*, "Terahertz and infrared spectroscopy of gated large-area graphene," *Nano Lett.*, vol. 12, pp. 3711–3715, 2012.
[11] N. Jung, B. Kim, A. C. Crowther, N. Kim, C. Nuckolls, and L. Brus, "Optical reflectivity and Raman scattering in few-layer-thick graphene highly doped by K and Rb," *ACS Nano*, vol. 7, no. 5, pp. 5708–5716, 2011.
[12] X. Wang, Z. Cheng, K. Xu, H. K. Tsang, and J. B. Xu, "High-responsivity graphene/silicon-heterostructure waveguide photodetectors," *Nature Photon.*, vol. 7, pp. 888–891, 2013.
[13] X. Gan *et al.*, "Chip-integrated ultrafast graphene photodetector with high responsivity," *Nature Photon.*, vol. 7, pp. 883–887, 2013.
[14] C. H. Lui, K. F. Mak, J. Shan, and T. F. Heinz, "Ultrafast photoluminescence from graphene," *Phys. Rev. Lett.*, vol. 105, 2010, Art. no. 127404.

[15] W. T. Liu, S. W. Wu, P. J. Schuck, M. Salmeron, Y. R. Shen, and F. Wang, "Nonlinear broadband photoluminescence of graphene induced by femtosecond laser irradiation," *Phys. Rev. B*, vol. 82, 2010, Art. no. 081408(R).
[16] R. J. Stöhr, R. Kolesov, J. Pflaum, and J. Wrachtrup, "Fluorescence of laser-created electron-hole plasma in graphene," *Phys. Rev. B*, vol. 82, 2010, Art. no. 121408.
[17] T. Koyama *et al.*, "Near-infrared photoluminescence in the femtosecond time region in monolayer graphene on SiO_2," *ACS Nano*, vol. 7, pp. 2335–2343, 2013.
[18] A. Säynätjoki *et al.*, "Rapid large-area multiphoton microscopy for characterization of graphene," *ACS Nano*, vol. 7, pp. 8441–8446, 2013.
[19] Y. D. Kim *et al.*, "Bright visible light emission from graphene," *Nature Nanotechnol.*, vol. 10, pp. 676–681, 2015.
[20] K. Liu *et al.*, "Bright multicolored photoluminescence of hybrid graphene/silicon optoelectronics," *ACS Photon.*, vol. 2, pp. 797–804, 2015.
[21] S. Y. Hong, J. I. Dadap, N. Petrone, P. C. Yeh, J. Hone, and R. M. Osgood Jr., "Optical third-harmonic generation in graphene," *Phys. Rev. X*, vol. 3, 2013, Art. no. 021014.
[22] J. Grandidier, D. M. Callahan, J. N. Munday, and H. A. Atwater, "Light absorption enhancement in thin-film solar cells using whispering gallery modes in dielectric nanospheres," *Adv. Mater.*, vol. 23, pp. 1272–1276, 2011.
[23] I. Calizo, I. Bejenari, M. Rahman, G. Liu, and A. A. Balandin, "Ultraviolet Raman microscopy of single and multilayer graphene," *J. Appl. Phys.*, vol. 106, 2009, Art. no. 043509.
[24] D. Brida *et al.*, "Ultrafast collinear scattering and carrier multiplication in graphene," *Nature Commun.*, vol. 4, 2013, Art. no. 1987.
[25] M. Mittendor *et al.*, "Carrier dynamics in Landau-quantized graphene featuring strong Auger scattering," *Nature Phys.* vol. 11, pp. 75–81, 2015.
[26] I. Gierz1 *et al.*, "Snapshots of non-equilibrium Dirac carrier distributions in graphene," *Nature Mater.*, vol. 12, pp. 1119–1124, 2013.
[27] E. Hendry, P. J. Hale, J. Moger, A. K. Savchenko, and S. A. Mikhailov, "Coherent nonlinear optical response of graphene," *Phys. Rev. Lett.*, vol. 105, 2010, Art. no. 097401.
[28] N. Kumar *et al.*, "Third harmonic generation in graphene and few-layer graphite films," *Phys. Rev. B*, vol. 87, 2013, Art. no. 121406(R).
[29] K. Liu *et al.*, "Ultra-fast pulse propagation in nonlinear graphene/silicon ridge waveguide," *Sci. Rep.*, vol. 5, pp. 16734–16734, 2015.
[30] S. Boubanga-Tombet, S. Chan, T. Watanabe, A. Satou, V. Ryzhii, and T. Otsuji, "Ultrafast carrier dynamics and terahertz emission in optically pumped graphene at room temperature," *Phys. Rev. B*, vol. 85, 2012, Art. no. 035443.
[31] T. Watanabe *et al.*, "The gain enhancement effect of surface plasmon polaritons on terahertz stimulated emission in optically pumped monolayer graphene," *New J. Phys.*, vol. 15, 2013, Art. no. 075003.
[32] M. V. Entin, L. I. Magarill, and D. L. Shepelyansky, "Theory of resonant photon drag in monolayer graphene," *Phys. Rev. B*, vol. 81, 2010, Art. no. 165441.
[33] Y. Bahk *et al.*, "Plasmon enhanced terahertz emission from single layer graphene," *ACS Nano*, vol. 8, pp. 9089–9096, 2014.
[34] J. Maysonnave *et al.*, "Room temperature broadband coherent terahertz emission induced by dynamical photon drag in graphene," *Nano Lett.*, vol. 14, pp. 5797–5802, 2014.
[35] V. E. Babicheva, S. V. Zhukovsky, R. S. Ikhsanov, I. E. Protsenko, I. V. Smetanin, and A. Uskov, "Hot electron photoemission from plasmonic nanostructures: The role of surface photoemission and transition absorption," *ACS Photon.*, vol. 2, pp. 1039–1048, 2015.
[36] Z. Fang *et al.*, "Plasmon-induced doping of graphene," *ACS Nano*, vol. 6, pp. 10222–10228, 2012.
[37] T. Zhang *et al.*, "Macroscopic and direct light propulsion of bulk graphene material," *Nature Photon.,* vol. 9, pp. 471–476, 2015.
[38] L. Prechtel *et al.*, "Time-resolved ultrafast photocurrents and terahertz generation in freely suspended graphene," *Nature Commun.*, vol. 3, 2012, Art. no. 646.
[39] A. Rustagi and C. J. Stanton, "Terahertz radiation from accelerating charge carriers in graphene under ultrafast photoexcitation," *Phys. Rev. B*, vol. 94, 2016, Art. no. 195207.
[40] H. F. Yuan, S. Khatua, P. Zijlstra, M. Yorulmaz, and O. Michel, "Thousand-fold enhancement of single-molecule fluorescence near a single gold nanorod," *Angew. Chem. Int. Ed.*, vol. 52, pp. 1217–1221, 2013.
[41] M. Lippitz, A. Dijk, and O. Michel, "Third-harmonic generation from single gold nanoparticles," *Nano Lett.*, vol. 5, pp. 799–802, 2005.
[42] W. Strek *et al.*, "Laser-induced white-light emission from graphene ceramics–opening a band gap in graphene," *Light: Science Appl.*, vol. 4, e237, 2015.